Neuroradiology (2023) 65:1063–1071
https://doi.org/10.1007/s00234-023-03145-6

PAEDIATRIC NEURORADIOLOGY

Whole-tumor histogram analysis of diffusion and perfusion metrics for noninvasive pediatric glioma grading

Yan Su[1] · Jie Kang[1] · Xiang Lin[1] · Dejun She[1] · Wei Guo[1] · Zhen Xing[1] · Xiefeng Yang[1] · Dairong Cao[1,2,3]

Received: 1 November 2022 / Accepted: 29 March 2023 / Published online: 3 April 2023

Abstract

Purpose An accurate assessment of the World Health Organization grade is vital for patients with pediatric gliomas to direct treatment planning. We aim to evaluate the diagnostic performance of whole-tumor histogram analysis of diffusion-weighted imaging (DWI) and dynamic susceptibility contrast-enhanced perfusion-weighted imaging (DSC-PWI) for differentiating pediatric high-grade gliomas from pediatric low-grade gliomas.

Methods Sixty-eight pediatric patients (mean age, 10.47 ± 4.37 years; 42 boys) with histologically confirmed gliomas underwent preoperative MR examination. The conventional MRI features and whole-tumor histogram features extracted from apparent diffusion coefficient (ADC) and cerebral blood volume (CBV) maps were analyzed, respectively. Receiver operating characteristic curves and the binary logistic regression analysis were performed to determine the diagnostic performance of parameters.

Results For conventional MRI features, location, hemorrhage and tumor margin showed significant difference between pediatric high- and low-grade gliomas (all, $P < .05$). For advanced MRI parameters, ten histogram features of ADC and CBV showed significant differences between pediatric high- and low-grade gliomas (all, $P < .05$). The diagnostic performance of the combination of DSC-PWI and DWI (AUC = 0.976, sensitivity = 100%, NPV = 100%) is superior to conventional MRI or DWI model, respectively ($AUC_{cMRI} = 0.700$, $AUC_{DWI} = 0.830$; both, $P < .05$).

Conclusion The whole-tumor histogram analysis of DWI and DSC-PWI is a promising method for grading pediatric gliomas.

Keywords Diffusion-weighted imaging · Dynamic susceptibility contrast-enhanced perfusion-weighted imaging · Pediatric gliomas · Histogram analysis

Introduction

Pediatric gliomas are the most common pediatric intracranial tumors. Pediatric glioma is fundamentally different from adult glioma in divergent mechanisms and molecular genetic alterations of tumorigenesis [1, 2]. Thus, the 2021 World Health Organization (WHO) classification of tumors of the central nervous system has divided diffuse gliomas into adult-type and pediatric-type [3]. Pediatric low-grade gliomas (PLGGs) and pediatric high-grade gliomas (PHGGs) reportedly vary in outcomes and treatment. The prognosis of PHGGs was typically dismal (the 5-year overall survival of 5% for glioblastoma) [4]. Besides, PHGGs are generally treated with maximal surgical resection, chemotherapy and adjuvant radiation. PHGGs misdiagnosed as PLGGs may be treated insufficiently than necessary. So far, the reference standard for determining the WHO grade of pediatric gliomas is a pathological diagnosis of the tumor specimen. However, given the risk of postoperative complications and the specific location of tumors, the surgical resection or stereotactic biopsy is not suitable for all glioma patients. Therefore, a noninvasive method is urgently needed to resolve this problem.

✉ Dairong Cao
dairongcao@163.com

[1] Department of Radiology, The First Affiliated Hospital of Fujian Medical University, 20 Cha-Zhong Road, Fujian 350005 Fuzhou, China

[2] Department of Radiology, Fujian Key Laboratory of Precision Medicine for Cancer, the First Affiliated Hospital, Fujian Medical University, Fuzhou 350005, Fujian, China

[3] Department of Radiology, National Regional Medical Center, Binhai Campus of the First Affiliated Hospital, Fujian Medical University, Fuzhou 350212, Fujian, China

The MR technique, especially diffusion-weighted imaging (DWI) and dynamic susceptibility contrast-enhanced perfusion-weighted imaging (DSC-PWI), could be used as an auxiliary diagnostic method to accurately assess the WHO grade of gliomas [5–8]. However, the diagnostic ability of DWI and DSC-PWI metrics for distinguishing low- and high-grade gliomas is controversial [9–11]. The most probable reason is that a single region of interest (ROI) or multiple ROIs used in previous studies may result in potential information bias and poor repeatability. Furthermore, most prior studies about pediatric gliomas were performed according to the 2016 WHO classification; thus, the role of the DWI and DSC-PWI in grading pediatric gliomas based on the latest criterion remains uncertain.

Whole-tumor histogram analysis is an objective method to evaluate the tumor quantitatively, and it could vastly eliminate the potential measurement sampling error and reflect the heterogeneity of gliomas. Several studies have shown that the whole-tumor histogram analysis is superior to conventional ROI method for its objectivity, comprehensiveness, and repeatability [12–14]. This whole-tumor method has illustrated the ability to grade tumors, predict the genotypes of gliomas, and differential diagnosis of intracranial, pelvic, and pancreatic lesions [15–18]. Meanwhile, prior studies about diffusion- or perfusion-weighted imaging combined with histogram analysis in adults with gliomas have been widely explored; nonetheless, these data may be inappropriate for children [19, 20].

Thus, our study aims to evaluate the diagnostic accuracy of DWI and DSC-PWI MR imaging combined with histogram analysis for grading pediatric gliomas according to the latest 2021 WHO classification.

Methods

Patient selection

Our institutional review committee approved the study. Due to the retrospective nature of the investigation, informed consent has been waived for this study. Between April 2010 and December 2021, 85 pediatric patients with low-grade (WHO grade 1 or 2) or high-grade (WHO grade 3 or 4) gliomas were consecutively selected from our database. Inclusion criteria were as follows: (1) a histopathologic diagnosis of gliomas according to the WHO criteria. (2) patients' age less than 18 years old at diagnosis. Of these 85 patients, 17 were excluded for the following criteria: (1) some glioma specimens were lost and could not be reclassified (n = 5); (2) lack of preoperative DWI or DSC-PWI MR imaging (n = 9); (3) suboptimal images with severe artifacts (n = 3). A total of 68 patients with 47 low-grade and 21 high-grade gliomas were included in our retrospective study.

Image acquisition

All MR images were acquired by 3.0 T MR scanners (Magnetom Skyra/Verio, Siemens, Germany) with a 20-channel head matrix coil. Before DSC-PWI images acquisition, a small preload dose of gadobenate dimeglumine (Gd-BOPTA) was administered to reduce the leakage effects. The DSC-PWI images were obtained during the first three phases before injecting the contrast material to establish a pre-contrast baseline. In the fourth phase, a bolus of Gd-BOPTA was injected for the scan. The bolus injection rate was 5 ml/s, and the standard dose was 0.1 mmol/kg, followed by a 20 mL continuous saline flush at the same rate. Details regarding the MR protocols used are shown in Table 1.

Table 1 MRI sequence parameters

Parameters	T2WI	T2-FLAIR	T1WI/CE-T1WI	DWI	DSC-PWI
TR (ms)	6000	9000/8500	250	8200/4600	1500/1600
TE (ms)	96/125	94/81	2.48/2.46	102/65	30
FA (degree)	150/90	150	70	180	90
FOV (mm^2)	220×220	220×220	220×220	220×220	220×220
ST (mm)	5	5	5	5	5
b-value (s/mm^2)	/	/	/	0, 1000	/
Matrix	384×384/ 320×320	256×256/ 320×320	256×256/ 320×320	192×192	128×128

TR, time of repeatation; TE, time of echo; FA, flip angle; FOV, field of view; ST, section thickness; T2WI, T2 weighted imaging; T2-FLAIR, T2-fluid attenuated inversion recovery; T1WI, T1 weighted imaging; CE-T1WI, contrast-enhanced T1 weighted imaging; DWI, diffusion-weighted imaging; DSC-PWI, dynamic susceptibility contrast-enhanced perfusion-weighted imaging

Image processing

ADC map was calculated automatically by the MRI system. DSC-PWI were post-processed on an image processing workstation (the Syngovia MR B19 version). DSC-PWI-derived whole-brain CBV maps were generated using an automated arterial input function and a single-compartment model.

Qualitative image analysis

All MR imaging evaluations were performed in the Siemens workstation (the Syngovia MR B19 version). Two neuroradiologists, who were blinded to the pathological results, evaluated all conventional MRI images independently (observer 1 and observer 2, with 5 and 10 years of experience in pediatric neuroradiology, respectively). The cMRI features evaluated in our study include: (1) tumor location (frontal, temporal, insular, parietal, occipital, brain stem, cerebellum, basal ganglia, or others); (2) enhancement (none, mild, or marked); (3) necrosis or cysts; (4) hemorrhage; (5) T1/FLAIR ratio (expansive, mixed, or infiltrative); (6) peritumoral edema; (7) crosses midline; (8) clear margin. The cMRI features were defined according to the Visually Accessible Rembrandt Images (VASARI) imaging criteria [21].

Quantitative image analysis

Two neuroradiologists drew the VOI that contained the solid component of whole-tumor (exclude cystic, necrotic, hemorrhagic, or blood vessel areas) on T2WI, referring to T2-FLAIR, T1WI, and CE-T1WI (3D slicer, version 4.8.1, http://slicer.org/). The ADC and CBV maps were coregistered to T2WI using SPM8 with a normalized mutual information cost function and 3rd Degree B-Spline interpolation (http://www.fil.ion.ucl.ac.uk/spm/). Then they were resampled referring to T2WI (Resample Image, 3D slicer). The VOI was moved to the ADC and CBV maps (Fig. 1). Histogram analysis was carried out using Slicer Radiomics (https://discourse.slicer.org/c/community/radiomics). All the post-processing software is open-source and easily obtained. The following features were extracted from the ADC and CBV histogram: (1) mean; (2) median; (3) 10th percentage; (4) 90th percentage; (5) interquartile range (IQR); (6) kurtosis, which is a metric of the degree of peakedness of a distribution; (7) skewness, which could describe the degree

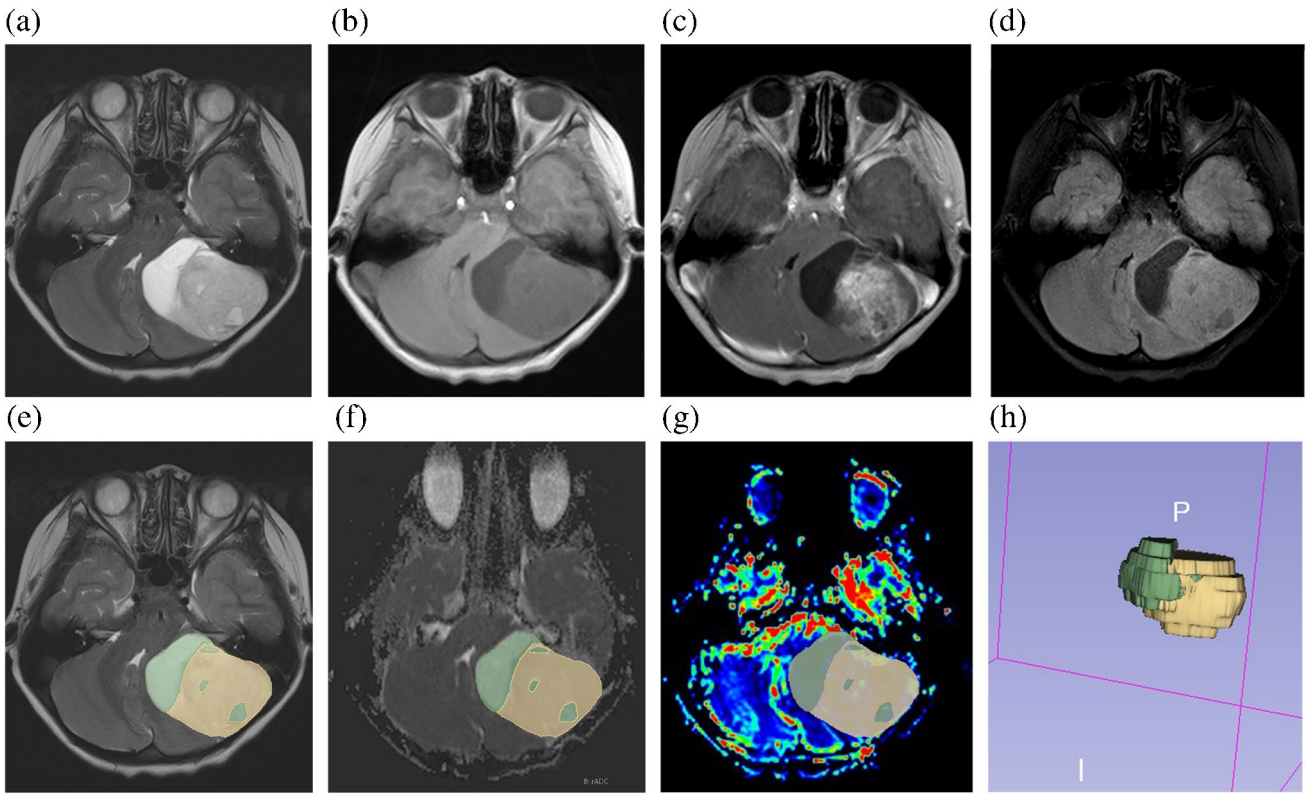

Fig. 1 According to the T2WI, T1WI, CE-T1WI, and T2FLAIR images (**a**-**d**), the VOI of the solid component (the yellow area) is drawn on T2WI (**e**) (exclude cystic, necrotic, hemorrhagic, or blood vessel areas, the green area) and registered to the ADC (**f**) and CBV images (**g**). The three-dimensional image of tumor segmentation is demonstrated on (**h**)

of asymmetry of a distribution; (8) entropy. The relative value of all quantitative MR parameters was calculated by dividing the value of the tumor by the reference value of the contralateral normal-appearing white matter. The time required for the whole-tumor histogram analysis method was 210.35 ± 33.88 s.

Statistical analysis

All statistical analyses were carried out by using SPSS (version 25.0, IBM, Armonk, NY, USA), MedCalc (version 15.2.2 MedCalc Software bvba, Ostend, Belgium), and GraphPad Prism (version 8.0.2, GraphPad Software, San Diego, Calif). All *P*-values less than 0.05 were considered statistically significant.

The chi-square test and Fisher's exact test were used for two-group comparisons of sex and cMRI characteristics, and the comparison of histogram features was performed with the Mann–Whitney *U* test. Receiver operating characteristic (ROC) curve analysis and the binary logistic regression analysis were constructed to evaluate the diagnostic accuracy. The Youden index (YI) was used to determine the cut-off value. The sensitivity, specificity, negative predictive value (NPV), and positive predictive value (PPV) were calculated. The area under the ROC curves (AUCs) among parameters were compared using the DeLong method with a Bonferroni correction for assessing the superiority of univariate and multivariate MR parameters.

The Cohen's Kappa and intraclass correlation coefficients (ICC) were used to assess the reliability of categorical and measurement data. Kappa or ICC values of > 0.75 indicated excellent agreement.

Table 2 Comparison of demographic and conventional MRI characteristics between pediatric low-grade gliomas from high-grade gliomas

Characteristics	PLGG(n = 47)	PHGG(n = 21)	*P*-value
Demography			
Age (years) ± SD	10.63 ± 4.45	10.10 ± 4.26	.64
Male sex (%)	27/47 (57.45)	15/21 (71.43)	.27
Location (No.)			< .001*
Frontal lobe	6	1	
Temporal lobe	3	0	
Insular lobe	0	0	
Parietal lobe	5	3	
Occipital lobe	1	0	
Brain stem	7	8	
Cerebellum	21	1	
Basal ganglia	1	8	
Others	3	0	
Enhancement (No.)			.15
None	9	2	
Mild	6	12	
Marked	32	7	
Necrosis or cysts (No.) (%)	31/47 (65.96)	9/21 (42.86)	.07
Hemorrhage (No.) (%)	5/47 (10.64)	7/21 (33.33)	.04*
T1/FLAIR ratio (No.)			.15
Expansive	35	15	
Mixed	11	3	
Infiltrative	1	3	
Peritumoral edema (No.) (%)	29/47 (61.70)	10/21 (47.62)	.68
Crosses midline (No.) (%)	5/47 (10.64)	5/21 (23.81)	.26
Clear margin (No.) (%)	45/47 (95.74)	15/21 (71.43)	.01*

*mean *P*-values no more than .05; cMRI, conventional MR imaging; PLGG, pediatric low-grade glioma; PHGG, pediatric high-grade glioma

Results

The results of the comparison in demographic and cMRI characteristics between PLGGs and PHGGs are shown in Table 2. PLGGs were more frequent in the cerebellar hemisphere than PHGGs ($P < 0.001$). PHGGs were more likely to demonstrate hemorrhage and unclear margin than PLGGs

Table 3 Comparison of histogram metrics derived from DWI and DSC-PWI between pediatric low-grade gliomas from high-grade gliomas

Parameters	PLGG(n = 47)	PHGG(n = 21)	*P*-value
DWI-related parameters			
$rADC_{mean}$	2.09 ± 0.55	1.47 ± 0.37	< .001*
$rADC_{median}$	2.06 ± 0.59	1.45 ± 0.40	< .001*
$rADC_{10th}$	1.76 ± 0.59	1.23 ± 0.31	< .001*
$rADC_{90th}$	2.41 ± 0.60	1.70 ± 0.44	< .001*
$rADC_{IQR}$	5.61 ± 3.59	4.53 ± 2.29	.41
$rADC_{kurtosis}$	1.47 ± 0.79	2.04 ± 1.90	.29
$rADC_{skewness}$	2.63 ± 7.90	-0.29 ± 6.42	.36
$rADC_{entropy}$	1.72 ± 0.32	1.67 ± 0.28	.78
DSC-PWI-related parameters			
$rCBV_{mean}$	2.05 ± 1.03	5.27 ± 3.21	< .001*
$rCBV_{median}$	1.78 ± 0.99	4.58 ± 2.92	< .001*
$rCBV_{10th}$	1.10 ± 3.02	5.12 ± 6.53	< .001*
$rCBV_{90th}$	2.75 ± 1.47	6.12 ± 3.56	< .001*
$rCBV_{IQR}$	3.93 ± 2.83	7.09 ± 5.33	< .001*
$rCBV_{kurtosis}$	2.08 ± 1.19	3.09 ± 2.65	.21
$rCBV_{skewness}$	3.40 ± 7.80	-1.44 ± 29.73	.61
$rCBV_{entropy}$	1.48 ± 0.31	1.86 ± 0.35	< .001*

Unless otherwise specified, data are means ± standard deviations; *mean *P*-values no more than .05; PLGG, pediatric low-grade glioma; PHGG, pediatric high-grade glioma; DWI, diffusion-weighted imaging; DSC-PWI, dynamic susceptibility contrast-enhanced perfusion-weighted imaging; rADC, relative apparent diffusion coefficient; rCBV, relative cerebral blood volume; 10th, 10th percentage; 90th, 90th percentage; IQR, interquartile range

(both, $P < 0.05$). There were no significant differences in sex, age, and other cMRI characteristics.

The advanced MR parameters of each pediatric glioma type are demonstrated in Table S1. The pilocytic astrocytomas accounted for 57.45% (27/47) of the pediatric low-grade gliomas. Table 3 summarizes the comparison of histogram metrics derived from ADC and CBV between PLGGs and PHGGs. For advanced MR parameters, ten histogram features of ADC and CBV showed significant differences between PLGGs and PHGGs (Fig. 2 and 3). Our study further found that the 90th value of ADC of the pilocytic astrocytomas was significantly higher than PHGGs and other PLGGs, respectively (both, $P_{corrected} < 0.01$; the corrected *P*-value was calculated by multiplying the uncorrected *P*-value by 3). Meanwhile, the 90th value of ADC of PLGGs was significantly higher than PHGGs ($P_{corrected} < 0.01$).

As shown in Table 4, according to ROC curve analysis, these ten histogram features were useful in grading pediatric gliomas (AUC = 0.752 - 0.911). The diagnostic performance of histogram metrics derived from diffusion and perfusion parameters was similar ($P_{corrected} > 0.05$, compared with each other; the corrected *P*-value was calculated by multiplying the uncorrected *P*-value by 45). The $rCBV_{entropy}$ showed the highest sensitivity and NPV (100% and 100%, respectively) among the histogram metrics, and the $rCBV_{10th}$ demonstrated the highest specificity (91.5%).

The optimal cutoff, YI, sensitivity, specificity, PPV, NPV, and AUC of all logistic regression models are reported in Table 5. Table S2 summarizes the comparative results of the single and combined logistic regression models for separating different pediatric glioma types (Fig. 4).

For the combined logistic regression models, the combination of DSC-PWI and DWI, which showed the highest

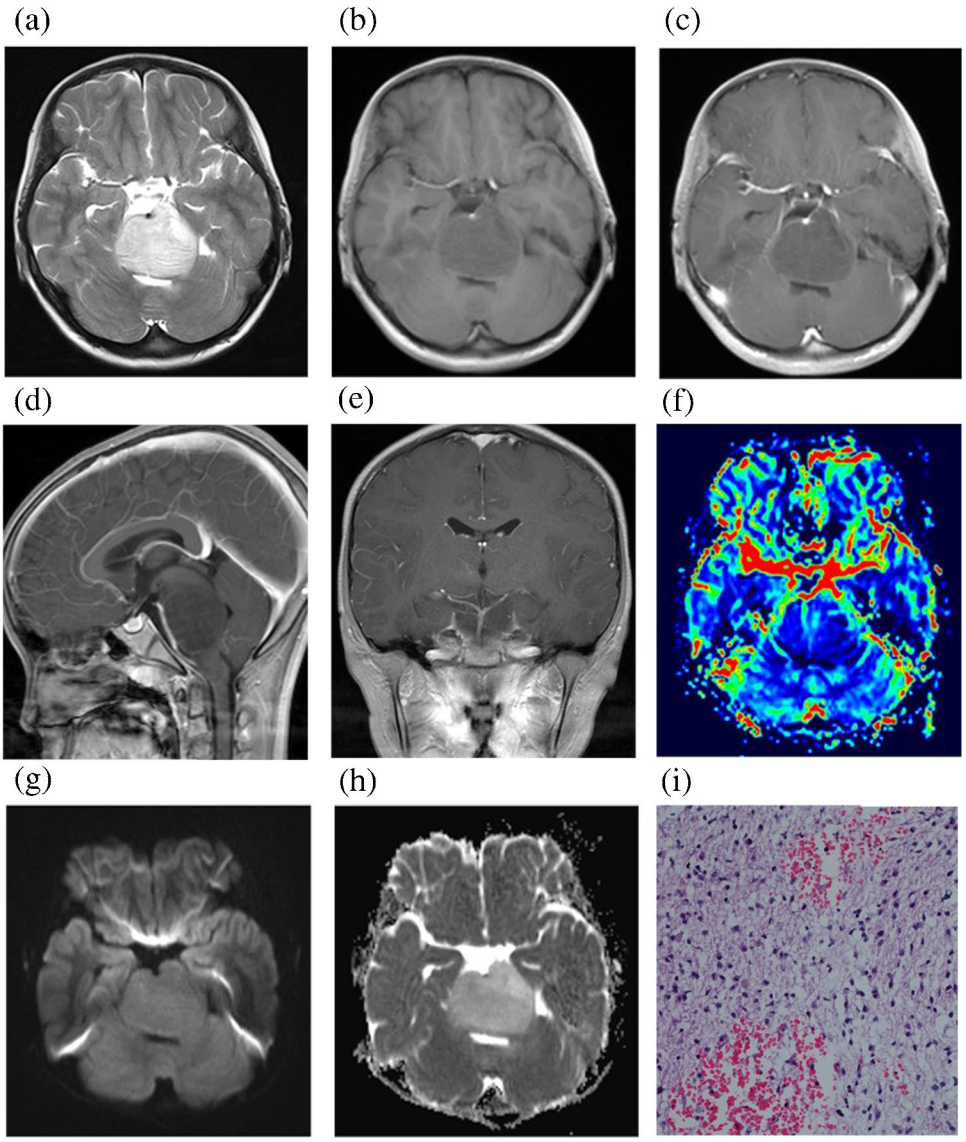

Fig. 2 An 8-year-old girl with a diffuse astrocytoma in the brain stem (WHO grade 2). The tumor demonstrates hyperintensity on the T2WI (**a**), hypointensity on the T1WI (**b**), and no enhancement on the postcontrast T1WI (**c**-**e**). The tumor demonstrates isointensity on the DWI (**g**). The tumor shows slight hypointensity on the CBV map (**f**) and hyperintensity on the ADC map (**h**), with relative mean values of 2.12 and 1.41, respectively. The image of hematoxylin–eosin staining (H & E) is demonstrated on (**i**)

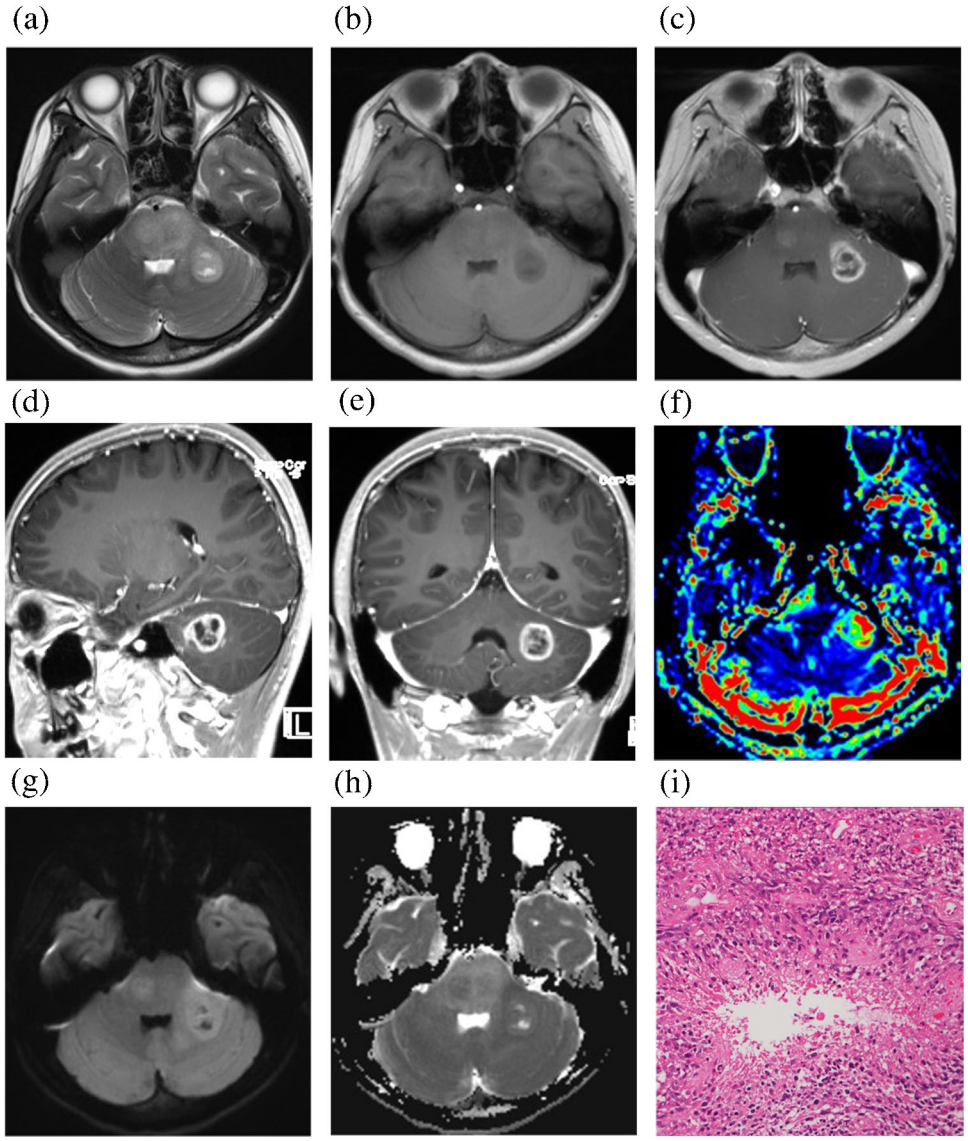

Fig. 3 An 11-year-old girl with diffuse midline glioma in the brain stem (WHO grade 4). The tumor demonstrates slight hyperintensity on the T2WI (**a**), hypointensity on the T1WI (**b**), and partly obvious enhancement on the postcontrast T1WI (**c**-**e**). The tumor demonstrates partial hyperintensity on the DWI (**g**). The tumor shows partly obvious hyperintensity on the CBV map (**f**) and hypointensity on the ADC map (**h**), with relative mean values of 1.42 and 4.11, respectively. The image of hematoxylin–eosin staining (H & E) is demonstrated on (**i**)

Table 4 Diagnostic performance of histogram metrics derived from DWI and DSC-PWI MR imaging for differentiating pediatric low-grade gliomas from high-grade gliomas

Parameter	Cut-off value	YI	Sen (%)	Spe (%)	PPV (%)	NPV (%)	AUC
$rADC_{mean}$	1.507	0.608	71.4	89.4	75.0	87.5	0.840
$rADC_{median}$	1.490	0.544	71.4	83.0	65.2	86.7	0.818
$rADC_{10th}$	1.232	0.539	66.7	87.2	70.7	85.4	0.810
$rADC_{90th}$	2.236	0.548	95.2	59.6	51.3	96.6	0.830
$rCBV_{mean}$	2.536	0.692	90.5	78.7	65.5	94.9	0.911
$rCBV_{median}$	1.971	0.607	90.5	70.2	57.6	94.3	0.877
$rCBV_{10th}$	1.731	0.629	71.4	91.5	78.9	87.8	0.828
$rCBV_{90th}$	4.210	0.587	71.4	87.2	71.4	87.2	0.861
$rCBV_{IQR}$	3.220	0.415	90.5	51.1	45.2	92.3	0.752
$rCBV_{entropy}$	1.484	0.553	100.0	55.3	50.0	100.0	0.798

DWI, diffusion-weighted imaging; DSC-PWI, dynamic susceptibility contrast-enhanced perfusion-weighted imaging; PLGG, pediatric low-grade glioma; PHGG, pediatric high-grade glioma; YI, Youden index, Sen, sensitivity, Spe, specificity, PPV, positive predictive value, NPV, negative predictive value, AUC, area under the curves; rADC, relative apparent diffusion coefficient; rCBV, relative cerebral blood volume; 10th, 10th percentage; 90th, 90th percentage; IQR, interquartile range

Table 5 The diagnostic performance of all logistic regression models for grading pediatric gliomas

Logistic regression models	YI	Sen (%)	Spe (%)	PPV (%)	NPV (%)	AUC
cMRI	0.375	52.4	85.1	61.1	80.0	0.700
DWI	0.548	95.2	59.6	51.4	96.6	0.830
DSC-PWI	0.692	90.5	78.7	65.5	94.9	0.911
DSC-PWI + DWI	0.851	100.0	85.1	75.0	100.0	0.976
DSC-PWI + DWI + cMRI	0.851	100.0	85.1	75.0	100.0	0.976

YI, Youden index; Sen, sensitivity; Spe, specificity; PPV, positive predictive value; NPV, negative predictive value; AUC, area under the curves; cMRI, conventional MR imaging; DWI, diffusion-weighted imaging; DSC-PWI, dynamic susceptibility contrast-enhanced perfusion-weighted imaging. The logistic regression equation for single and combined MR parameters models are as follows: logit (p) $_{cMRI}$ = [-1.409 + (1.481 * hemorrhage) + (2.241 * clear margin)], logit (p) $_{DWI}$ = [4.030 + (-2.371 * $rADC_{90th}$)], logit (p) $_{DSC\text{-}PWI}$ = [-5.123 + (1.410 * $rCBV_{mean}$)], logit (p) $_{DSC\text{-}PWI+DWI}$ = [1.252 + (-8.480 * $rCBV_{median}$) + (10.252 * $rCBV_{mean}$) + (-5.459 * $rADC_{90th}$)], and logit (p) $_{DSC\text{-}PWI+DWI+cMRI}$ = [1.252 + (-8.480 * $rCBV_{median}$) + (10.252 * $rCBV_{mean}$) + (-5.459 * $rADC_{90th}$)]

AUC, sensitivity, and NPV (0.976, 100%, and 100%, respectively), is superior to the cMRI or DWI model, respectively (AUC_{cMRI} = 0.700, AUC_{DWI} = 0.830; both, $P < 0.05$). However, the model of advanced MR techniques combined with cMRI could not further improve the diagnostic ability for grading pediatric gliomas ($P = 1.00$). Inter-observer measurements showed a good agreement (all, ICC/Kappa > 0.75).

Discussion

Different from the adult-type gliomas, the tumor types of pediatric gliomas we encounter in clinical practice are widely heterogeneous, and evaluating tumor grading is the first and essential step. Our study found that whole-tumor histogram features derived from ADC and CBV could be used to differentiate PHGG from PLGG. The combination of DWI and DSC-PWI MR imaging shows the highest diagnostic ability for this differentiation.

Notably, although the cMRI could be used to differentiate PHGG from PLGG, the overlap of morphological features may decrease the sensitivity (52.4%) and the diagnostic accuracy (AUC = 0.700) of the cMRI. For example, despite the fact that PLGGs were more frequent in the cerebellar hemisphere than PHGGs, low-grade tumors that occurred in the midline (7/47, 14.89%) still be hard to identify. Advanced MR imaging methods are valuable to determine such tumors.

Regarding diffusion-weighted MR imaging parameters, $rADC_{mean}$, $rADC_{median}$, $rADC_{10th}$, and $rADC_{90th}$ values were significantly lower in the high-grade group than in the low-grade group (all, $P < 0.05$) in our research. That is in concordance with previous studies [22, 23]. A study by Yao et al. suggested a significant difference in mean and minimum ADC of PHGG versus PLGG [24]. Similar to adult-type glioma, the cellularity of high-grade pediatric glioma is higher than the low-grade tumor. In contrast, Server et al. revealed an extensive overlap in ADC values between these two tumors or no difference between them [11]. One possible reason was the small sample size of the low-grade group in the latter report, which was markedly less than the high-grade group (15 vs. 37). Regarding perfusion-weighted MR imaging parameters, $rCBV_{mean}$, $rCBV_{median}$, $rCBV_{10th}$, and $rCBV_{90th}$ were significantly higher in PHGGs compared to PLGGs in this study. A comprehensive meta-analysis revealed that the rCBV was larger in PHGG than in PLGG [25]. A multicenter report with a large sample showed that the 95th percentile of rCBV was significantly higher in high-grade

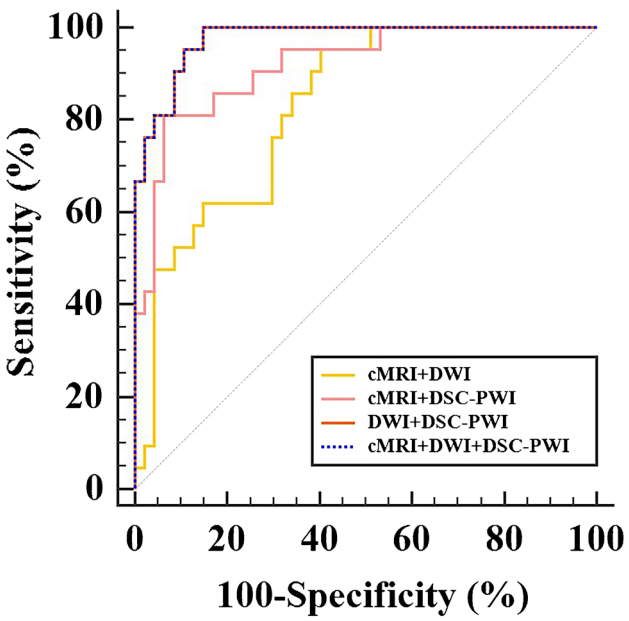

Fig. 4 Receiver operating characteristic of the single and combined logistic regression models for differentiating pediatric low- from high-grade gliomas

gliomas compared to low-grade gliomas [26]. Meanwhile, Falk et al. suggested that the 90th percentile of rCBV was significantly higher in grade 3 gliomas than in grade 2 [27]. The results of prior reports tie well with our results. Another valuable finding was that indicators of heterogeneity ($rCBV_{IQR}$ and $rCBV_{entropy}$) in PHGGs were significantly higher than PLGG. Sudre et al. found that the sum entropy, entropy, and difference entropy had a good ability for differentiating grade 2 gliomas from grade 4 gliomas, consistent with our results [26]. The extensive microvasculature heterogeneity and the distinct vascular gene expression signatures of gliomas might be associated with WHO grade [28].

The combination of DWI and DSC-PWI showed the highest accuracy in differentiating pediatric low- and high-grade gliomas. The AUC value of this multiple parameters model was higher than DSC-PWI-based single parameter model (0.911 vs. 0.976), although the difference was not significant. Interestingly, according to the logistic regression equation, we found that the most significant histogram metric among ADC-derived parameters was $rADC_{90th}$ rather than $rADC_{10th}$ or $rADC_{mean}$, which was the most widely used ADC-derived parameters. The result may be partly because ADC_{90th} of low-grade gliomas are significantly higher than high-grade tumor in our study. This finding needed to be verified by a more extensive sample study in the future.

Among the present study's limitations, we realize that the subtypes of gliomas in our study are extremely heterogeneous with low numbers, and it may affect the strength of results. Thus, a larger sample of individual glioma types is needed to verify these preliminary findings. Furthermore, we obtain MR data from two different 3.0 T MR scanners. Nevertheless, we optimized the MR sequences to minimize the difference and used the relative values to decrease the potential bias caused by individual differences. Finally, we find that a multicentered prospective investigation is warranted to ascertain the reproducibility of the preliminary conclusions in our single-center retrospective study.

Conclusions

The whole-tumor histogram analysis of DWI and DSC-PWI parameters is a promising method for grading pediatric gliomas.

Supplementary Information The online version contains supplementary material available at https://doi.org/10.1007/s00234-023-03145-6.

Funding This study was supported by the Leading Project of the Department of Science and Technology of Fujian Province (grant number 2020Y0025), the National Natural Science Foundation of China (grant number 82071869), and the Startup Fund for Scientific Research, Fujian Medical University (grant number 2018QH1048), the Young and Middle-aged Key Personnel Training Project of Fujian Provincial Health Commission (grant number 2021GGA025), and the Young and Middle-aged Key Personnel Training Project of Fujian Provincial Health Commission (grant number 2020GGA049s).

Data availability The datasets generated and/or analyzed during the current study are available from the corresponding author on reasonable request.

Compliance with ethical standards

Conflict of interest The authors declare that they have no conflict of interest.

Ethical approval All procedures performed in studies involving human participants were in accordance with the ethical standards of the institutional and/or national research committee and with the 1964 Helsinki declaration and its later amendments or comparable ethical standards.

For this type of study formal consent is not required.

Informed consent The study was approved by our institutional review committee. Informed consent was waived off due to the retrospective nature of the study.

References

1. Jones DT, Mulholland SA, Pearson DM et al (2011) Adult grade II diffuse astrocytomas are genetically distinct from and more aggressive than their pediatric counterparts. Acta Neuropathol 121:753–761. https://doi.org/10.1007/s00401-011-0810-6
2. Paugh BS, Qu C, Jones C et al (2010) Integrated molecular genetic profiling of pediatric high-grade gliomas reveals key differences with the adult disease. J Clin Oncol 28:3061–3068. https://doi.org/10.1200/JCO.2009.26.7252
3. Louis DN, Perry A, Wesseling P et al (2021) The 2021 WHO Classification of Tumors of the Central Nervous System: a summary. Neuro Oncol 23:1231–1251. https://doi.org/10.1093/neuonc/noab106
4. Kline C, Felton E, Allen IE, Tahir P, Mueller S (2018) Survival outcomes in pediatric recurrent high-grade glioma: results of a 20-year systematic review and meta-analysis. J Neurooncol 137:103–110. https://doi.org/10.1007/s11060-017-2701-8
5. Zhang HW, Lyu GW, He WJ et al (2020) DSC and DCE Histogram Analyses of Glioma Biomarkers, Including IDH, MGMT, and TERT, on Differentiation and Survival. Acad Radiol 27:e263–e271. https://doi.org/10.1016/j.acra.2019.12.010
6. Xing Z, Yang X, She D, Lin Y, Zhang Y, Cao D (2017) IDH Noninvasive Assessment of Mutational Status in World Health Organization Grade II and III Astrocytomas Using DWI and DSC-PWI Combined with Conventional MR Imaging. AJNR Am J Neuroradiol 38:1138–1144. https://doi.org/10.3174/ajnr.A5171
7. Patel P, Baradaran H, Delgado D et al (2017) MR perfusion-weighted imaging in the evaluation of high-grade gliomas after treatment: a systematic review and meta-analysis. Neuro Oncol 19:118–127. https://doi.org/10.1093/neuonc/now148
8. Morana G, Tortora D, Staglianò S et al (2018) Pediatric astrocytic tumor grading: comparison between arterial spin labeling and dynamic susceptibility contrast MRI perfusion. Neuroradiology 60:437–446. https://doi.org/10.1007/s00234-018-1992-6
9. You SH, Choi SH, Kim TM et al (2018) Differentiation of High-Grade from Low-Grade Astrocytoma: Improvement in Diagnostic

Accuracy and Reliability of Pharmacokinetic Parameters from DCE MR Imaging by Using Arterial Input Functions Obtained from DSC MR Imaging. Radiology 286:981–991. https://doi.org/10.1148/radiol.2017170764
10. Togao O, Hiwatashi A, Yamashita K et al (2016) Differentiation of high-grade and low-grade diffuse gliomas by intravoxel incoherent motion MR imaging. Neuro Oncol 18:132–141. https://doi.org/10.1093/neuonc/nov147
11. Server A, Kulle B, Gadmar ØB, Josefsen R, Kumar T, Nakstad PH (2011) Measurements of diagnostic examination performance using quantitative apparent diffusion coefficient and proton MR spectroscopic imaging in the preoperative evaluation of tumor grade in cerebral gliomas. Eur J Radiol 80:462–470. https://doi.org/10.1016/j.ejrad.2010.07.017
12. Zhu Q, Zou J, Ye J et al (2022) Comparative study of conventional ROI-based and volumetric histogram analysis derived from CT enhancement in differentiating malignant and benign renal tumors. Br J Radiol 95:20210801. https://doi.org/10.1259/bjr.20210801
13. Rezvani HR, Khoshpouri P, Ghadimi M et al (2020) Comparison between ROI-based and volumetric measurements in quantifying heterogeneity of liver stiffness using MR elastography. Eur Radiol 30:1609–1615. https://doi.org/10.1007/s00330-019-06478-0
14. Ahn SJ, Shin HJ, Chang JH, Lee SK (2014) Differentiation between primary cerebral lymphoma and glioblastoma using the apparent diffusion coefficient comparison of three different ROI methods. PLoS One 9:e112948. https://doi.org/10.1371/journal.pone.0112948
15. Gao A, Zhang H, Yan X et al (2022) Whole-Tumor Histogram Analysis of Multiple Diffusion Metrics for Glioma Genotyping. Radiology 302:652–661. https://doi.org/10.1148/radiol.210820
16. Vajapeyam S, Brown D, Ziaei A et al (2022) ADC Histogram Analysis of Pediatric Low-Grade Glioma Treated with Selumetinib: A Report from the Pediatric Brain Tumor Consortium. AJNR Am J Neuroradiol 43:455–461. https://doi.org/10.3174/ajnr.A7433
17. Xu Z, Yang L, Liu Q et al (2022) Machine Learning of Dose-Volume Histogram Parameters Predicting Overall Survival in Patients with Cervical Cancer Treated with Definitive Radiotherapy. J Oncol 2022:2643376. https://doi.org/10.1016/j.radonc.2020.11.030
18. De RR, Maris B, Cardobi N et al (2018) Can histogram analysis of MR images predict aggressiveness in pancreatic neuroendocrine tumors? Eur Radiol 28:2582–2591. https://doi.org/10.1007/s00330-017-5236-7
19. Sturm D, Pfister SM, Jones DTW (2017) Pediatric Gliomas: Current Concepts on Diagnosis, Biology, and Clinical Management. J Clin Oncol 35:2370–2377. https://doi.org/10.1200/JCO.2017.73.0242
20. Chiang JC, Ellison DW (2017) Molecular pathology of pediatric central nervous system tumours. J Pathol 241:159–172. https://doi.org/10.1002/path.4813
21. Cancer Imaging Archive website (2020) VASARI Research Project. https://www.wiki.cancerimagingarchive.net/display/Public/VASARI+Research+Project. Updated March 20, 2020. Accessed July 30, 2020.
22. Qi XX, Shi DF, Ren SX et al (2018) Histogram analysis of diffusion kurtosis imaging derived maps may distinguish between low and high grade gliomas before surgery. Eur Radiol 28:1748–1755. https://doi.org/10.1007/s00330-017-5108-1
23. Du N, Zhou X, Mao R et al (2022) Preoperative and Noninvasive Prediction of Gliomas Histopathological Grades and IDH Molecular Types Using Multiple MRI Characteristics. Front Oncol 12:873839. https://doi.org/10.3389/fonc.2022.873839
24. Yao R, Cheng A, Liu M, Zhang Z, Jin B, Yu H (2021) The Diagnostic Value of Apparent Diffusion Coefficient and Proton Magnetic Resonance Spectroscopy in the Grading of Pediatric Gliomas. J Comput Assist Tomogr 45:269–276. https://doi.org/10.1097/RCT.0000000000001130
25. Van SL, Kouwenberg V, Meijer F, Smits M, Henssen D (2022) A systematic review and meta-analysis on the differentiation of glioma grade and mutational status by use of perfusion-based magnetic resonance imaging. Insights Imaging 13:102. https://doi.org/10.1186/s13244-022-01230-7
26. Sudre CH, Panovska-Griffiths J, Sanverdi E et al (2020) Machine learning assisted DSC-MRI radiomics as a tool for glioma classification by grade and mutation status. BMC Med Inform Decis Mak 20:149. https://doi.org/10.1186/s12911-020-01163-5
27. Falk A, Fahlström M, Rostrup E et al (2014) Discrimination between glioma grades II and III in suspected low-grade gliomas using dynamic contrast-enhanced and dynamic susceptibility contrast perfusion MR imaging: a histogram analysis approach. Neuroradiology 56:1031–1038. https://doi.org/10.1007/s00234-014-1426-z
28. Zhang L, He L, Lugano R et al (2018) IDH mutation status is associated with distinct vascular gene expression signatures in lower-grade gliomas. Neuro Oncol 20:1505–1516. https://doi.org/10.1093/neuonc/noy088